

**Life Cycle Cost-Based Optimization Framework for Seismic Design and Quantifying
Target Safety of Dual Steel Buildings with Buckling-Restrained Braces**

(Supplementary Document)

Prepared by

Hossein Ahmadie Amiri, Homayoon E. Estekanchi

Sharif University of Technology, Tehran, Iran

September, 2022

Supplementary Details of Building Performance Model

This section provides full details of the building performance model for seismic loss estimation and Life Cycle Cost (LCC)-based design using FEMA P-58 methodology.

Table S1: Required parameters for estimating seismic losses in the studied buildings using FEMA P-58 methodology

Parameter ^a	Value ^b
1. Number of seismic intensity levels for loss estimation	10, same as Fig. S1
2. Number of realizations in each seismic intensity level for Monte Carlo simulation	1000
3. Total dispersion of peak drift and peak acceleration in Monte Carlo simulation	$\beta = \sqrt{\beta_{nr}^2 + \beta_m^2}$ according to Eq. (2) of the paper
3.1. Record-to-Record dispersion, β_{rr}	0.354
3.2. Modeling dispersion ($\beta_m = \sqrt{\beta_c^2 + \beta_q^2} \leq 0.5$)	0.25, assuming average quality
3.2.1. Dispersion for construction quality assurance, β_c	0.25, assuming average quality
3.2.2. Dispersion for quality of nonlinear analytical model, β_q	0.25, assuming average quality
4. Total dispersion of maximum residual drift in Monte Carlo simulation when simplified analysis is used	0.8
5. Lower bound of total dispersion for collapse capacity	0.6
6. Time-dependent population model	
6.1. Peak population for commercial office occupancy	4 person/1000 ft ²
6.2. Dispersion of peak population in different realizations	0.2
6.3. Time-dependent variation of peak population (peak population \times hourly factor \times monthly factor)	as in Fig. S2
7. Maximum worker for building repair	1 person/1000 ft ²
8. Dispersion of maximum worker in different realizations	0.2
9. Expected lifetime of the building, T	50 years
10. Annual discount rate, r	3%
11. Total loss threshold	50%
12. Average of building replacement cost	3000 \$/m ² + Cost of beams, columns, and BRBs 1900 \$/m ² + Cost of beams, columns, and BRBs
12.1. Construction cost	4.2 \$/kg according to Eq. (23) of the paper with $f_{BRB} = 8.4$ \$/kg
12.1.1. Perimeter frames (beams and columns) cost including 15% overhead for steel connections cost	1900 \$/m ²
12.1.2. BRBs cost	520 \$/m ²
12.1.3. Fixed construction cost (constant for all design alternatives in optimization process)	1900 \$/m ²
12.1.3.1. Cost of structural components other than beams, columns, and BRBs including gravity frames, pinned connections, column splices, column base plates	1380 \$/m ²
12.1.3.2. Cost of non-structural components including foundation, ceiling, roof, wall, facade, electrical and mechanical installations, architect/engineers/contractors fees, etc.	
12.2. Contents cost	750 \$/m ²
12.3. Cost of demolition and site clearance	350 \$/m ²
13. Dispersion of replacement cost in different realizations	0.2
14. Average of building replacement time	
14.1. 4-story building	392 days [1]
14.2. 8-story building	462 days [1]
14.3. 12-story building	550 days [1]
15. Dispersion of replacement time in different realizations	0.2
16. Cost corresponding to repair or replacement time	92.3 \$/m ² /month
16.1. Rental cost	50.0 \$/m ² /month [2]
16.2. Cost of relocation and reduced income	42.3 \$/m ² /month [3]
17. Average of collapse-induced injury rate	10%
18. Average of collapse-induced fatality rate	90%
19. Dispersion of casualty (injury and fatality) rate in different realizations	0.5
20. Cost per injury, f_{inj}	2.25E+04 \$/person [3]
21. Cost per fatality, f_{fat}	4.10E+06 \$/person [3]
22. Building irreparability fragility model based on maximum Residual Inter-story Drift Ratio (RIDR _{max})	
22.1. Average of irreparable RIDR _{max}	1%
22.2. Dispersion of irreparable RIDR _{max}	0.3

^a dispersion of the parameters refers to the log-normal standard deviation.

^b all cost data are adjusted to 2016 US dollars using RSMeans [4] to be consistent with component repair costs in FEMA P-58.

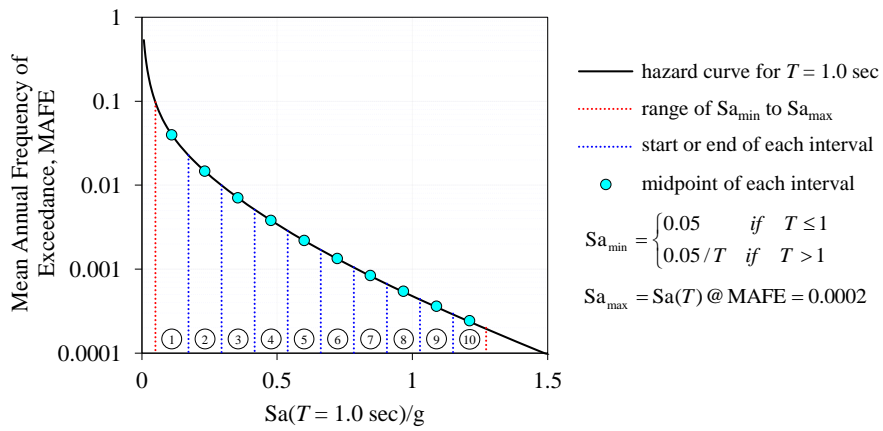


Fig. S1: Determining seismic intensity levels from the seismic hazard curve for a sample building with a fundamental period of 1 sec (as per the procedure given in FEMA P-58 [5])

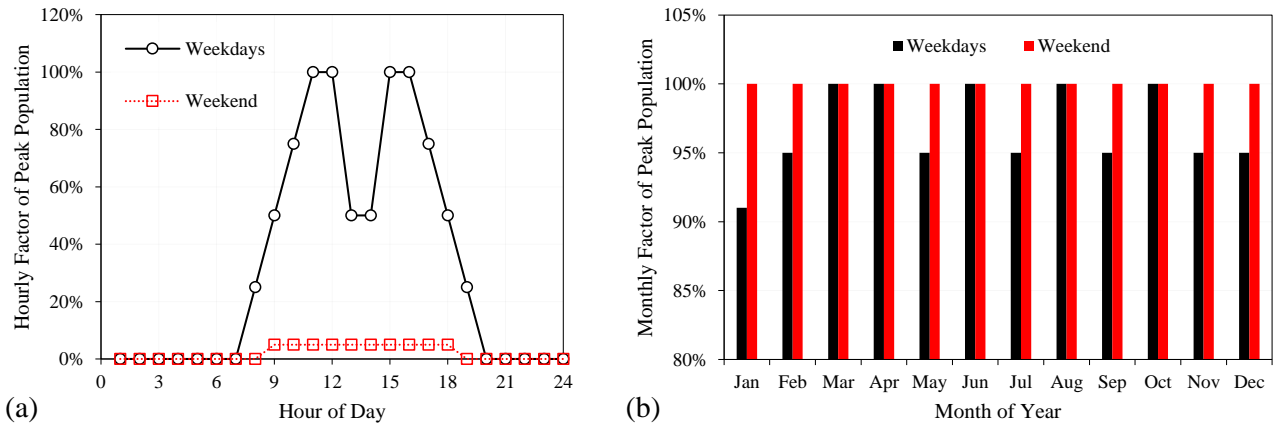


Fig. S2: Time-dependent variation of peak population for commercial office occupancies based on FEMA P-58 [5]: (a) hourly variation and (b) monthly variation

Table S2: Vulnerable structural and non-structural components in the studied buildings along with their location and normal quantity

Component Type ^{a,b}	Component Name	ID in FEMA P-58	Location	Unit ^c	Quantity per Location ^d	
					μ_{quant}	β_{quant}
SC	Bolted shear tab connection	B1031.001	Each Story	1 EA	96	0
	Column base plate	B1031.011(a-c)	Base	1 EA	16	0
	Welded column splices	B1031.021(a-c)	Odd Stories except Base	1 EA	16	0
	Post-Northridge welded moment connection other than RBS-one sided	B1035.(021&022)	Each story	1 EA	8	0
	Post-Northridge welded moment connection other than RBS-double	B1035.(031&032)	Each Story	1 EA	8	0
	Buckling Restrained Brace (Chevron Configuration)	B1033.101(a-c)	Each Story	1 Bay	4	0
NSC-D	Curtain walls	B2022.001	Each Story	30 ft ²	280	0.6
	Dry wall partition	C1011.001a	Each Story	100 ft	28	0.2
	Dry wall finishes	C3011.001a	Each Story	100 ft	28	0.7
	Prefabricated steel stair	C2011.001b	Each Story	1 EA	2	0.2
NSC-A	Raised access floor	C3027.001	Each Story	100 ft ²	105	0.2
	Suspended ceiling	C3032.001a	Each Story	250 ft ²	50.4	0.05
	Independent pendant lighting (seismically rated)	C3034.002	Each Story	1 EA	210	0.3
	Cold or hot potable water piping	D2021.011a	Each Story	1000 ft	0.59	0.7
	Fire sprinkler water piping	D4011.021a	Each Story	1000 ft	2.8	0.1
	Fire sprinkler drops	D4011.031a	Each Story	100 EA	1.26	0.2
	HVAC ducting (cross sectional area $\geq 6 \text{ ft}^2$)	D3041.012a	Each Story	1000 ft	0.28	0.2
	HVAC ducting (cross sectional area $< 6 \text{ ft}^2$)	D3041.011a	Each Story	1000 ft	1.05	0.2
	HVAC drops	D3041.031a	Each Story	10 EA	12.6	0.5
	Variable Air Volume box	D3041.041a	Each Story	10 EA	9.8	0.2
	Traction elevator	D1014.011	Base	1 EA	2	0.7
	Chiller	D3031.011a	Base	75 ton	0.5×nSt	0.1
	Low voltage switchgear	D5012.021a	Base	225 AP	0.01×nSt	0.4
	Motor control center	D5012.013a	Base	1 EA	0.5×nSt	0.5
	Concrete tile roof	B3011.011	Roof	100 ft ²	38	1.3
	Cooling tower	D3031.021a	Roof	75 ton	0.5×nSt	0.1
	Air handling unit	D3052.011a	Roof	4000 CFM	2.5×nSt	0.2

^a SC: Structural Component, NSC-D: Drift-sensitive Non-Structural Component, NSC-A: Acceleration-sensitive Non-Structural Component.

^b The non-structural vulnerable components and their normal quantity are adopted based on the normative quantity estimation tool provided in the third volume of FEMA P-58 [6].

^c EA: per unit, AP: Amper, CFM: ft³/minute.

^d β : Log-normal Standard Deviation, μ : Mean, nSt: Number of Story.

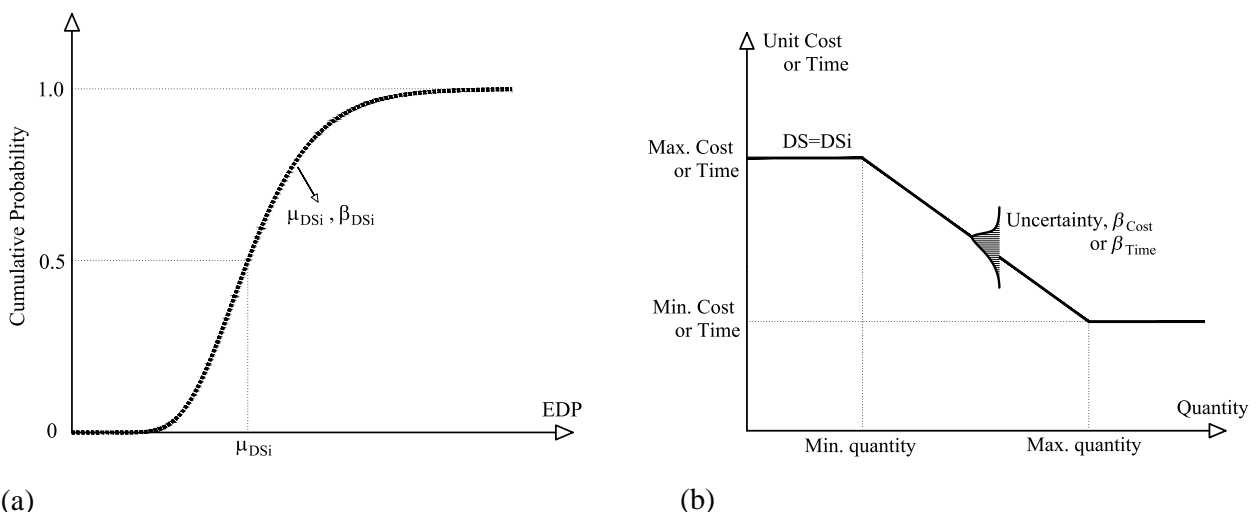


Fig. S3: Schematic representation of (a) component damage fragility model and (b) corresponding consequence model in FEMA P-58 methodology

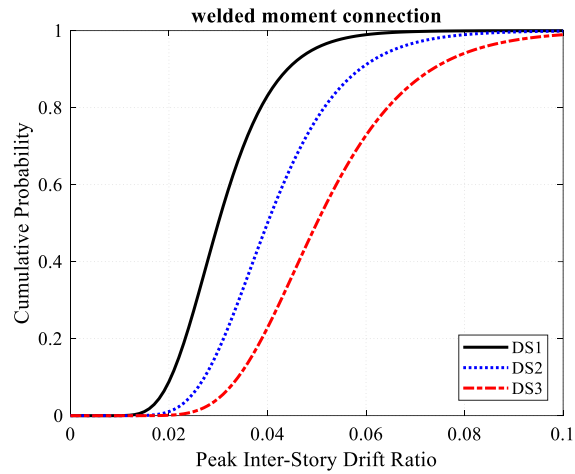
Table S3: Details of the damage fragility model and the corresponding consequence model for vulnerable components used

Components	Damage Fragility Model Parameters ^{a,b}					Consequence Model ^{a,b}													
	Name	Unit ^c	DS No.	μ_{DS}	β_{DS}	DS-Type	EDP	Repair Cost & Repair Time Parameters						Human Casualty Parameters					
								Min quantity	Max quantity	$\mu_{MaxCost}$ (\$)	$\mu_{MinCost}$ (\$)	β_{Cost}	$\mu_{MaxTime}$ (day-person)	$\mu_{MinTime}$ (day-person)	β_{Time}	Casualty Affected Area (ft ²)	$\mu_{InjuryRate}$	$\mu_{FatalityRate}$	β_{Casual}
Bolted shear tab connection	1 EA	1	0.04	0.4				5	20	0	0	0.25	0	0	0.35	0	0	0	0
		2	0.04	0.4	Seq(MutEx(DS1,DS2),DS3,DS4)		PIDR	5	20	16536	10176	0.37	16.0	9.9	0.45	0	0	0	0
		3	0.08	0.4				5	20	15564	11025	0.38	15.1	10.7	0.45	0	0	0	0
		4	0.11	0.4				5	20	15264	10812	0.38	14.8	10.5	0.46	0	0	0	0
Column base plate (WColumn ≤ 150 plf)	1 EA	1	0.04	0.4				5	20	0	0	0.25	0	0	0.35	0	0	0	0
		2	0.04	0.4	Seq(MutEx(DS1,DS2), DS3,DS4)		PIDR	5	20	25363	15608	0.41	24.6	15.1	0.48	0	0	0	0
		3	0.07	0.4				5	20	31464	2287	0.37	30.5	21.6	0.44	0	0	0	0
		4	0.10	0.4				5	20	36744	26027	0.34	35.7	25.3	0.42	0	0	0	0
Column base plate (150 < WColumn ≤ 300 plf)	1 EA	1	0.04	0.4				5	20	0	0	0.25	0	0	0.35	0	0	0	0
		2	0.04	0.4	Seq(MutEx(DS1,DS2),DS3,DS4)		PIDR	5	20	26403	16248	0.39	19.4	11.9	0.46	0	0	0	0
		3	0.07	0.4				5	20	33864	23987	0.34	24.9	17.6	0.42	0	0	0	0
		4	0.10	0.4				5	20	41544	29427	0.31	30.5	21.6	0.39	0	0	0	0
Column base plate (WColumn > 300 plf)	1 EA	1	0.04	0.4				5	20	0	0	0.25	0	0	0.35	0	0	0	0
		2	0.04	0.4	Seq(MutEx(DS1,DS2),DS3,DS4)		PIDR	5	20	27963	17208	0.37	18.5	11.4	0.45	0	0	0	0
		3	0.07	0.4				5	20	37464	26537	0.31	24.8	17.6	0.40	0	0	0	0
		4	0.10	0.4				5	20	47544	33677	0.27	31.5	22.3	0.37	0	0	0	0
Welded column splices (WColumn ≤ 150 plf)	1 EA	1	0.02	0.4				5	20	0	0	0.25	0	0	0.35	0	0	0	0
		2	0.02	0.4	Seq(MutEx(DS1,DS2),DS3)		PIDR	5	20	12142	7472	0.32	11.8	7.3	0.41	0	0	0	0
		3	0.05	0.4				5	20	13608	9639	0.30	13.2	9.4	0.39	0	0	0	0
		4	0.02	0.4	Seq(MutEx(DS1,DS2),DS3)		PIDR	5	20	13182	8112	0.30	9.7	6.0	0.39	0	0	0	0
Welded column splices (150 < WColumn ≤ 300 plf)	1 EA	1	0.02	0.4				5	20	16008	11339	0.27	11.8	8.3	0.37	0	0	0	0
		2	0.02	0.4	Seq(MutEx(DS1,DS2),DS3)		PIDR	5	20	14742	9072	0.27	9.8	6.0	0.37	0	0	0	0
		3	0.05	0.4				5	20	19608	13889	0.24	13.0	9.2	0.34	0	0	0	0
		4	0.02	0.4	Seq(MutEx(DS1,DS2),DS3)		PIDR	5	20	20880	13920	0.35	12.3	8.2	0.43	0	0	0	0
Post-Northridge welded moment connection other than RBS (beam one side, beam depth ≤ W27)	1 EA	1	0.03	0.3				3	7	35160	23440	0.31	20.7	13.8	0.39	0	0	0	0
		2	0.04	0.3	Seq(DS1,DS2,DS3)		PIDR	3	7	35160	23440	0.31	20.7	13.8	0.39	0	0	0	0
		3	0.05	0.3				3	7	35160	23440	0.31	20.7	13.8	0.39	0	0	0	0
		4	0.02	0.3	Seq(DS1,DS2,DS3)		PIDR	3	7	22080	14720	0.33	13.0	8.7	0.42	0	0	0	0
Post-Northridge welded moment connection other than RBS (beam one side, beam depth ≥ W30)	1 EA	1	0.03	0.3				3	7	38880	25920	0.28	22.9	15.2	0.38	0	0	0	0
		2	0.04	0.3	Seq(DS1,DS2,DS3)		PIDR	3	7	38880	25920	0.28	22.9	15.2	0.38	0	0	0	0
		3	0.05	0.3				3	7	42000	28000	0.34	24.7	16.5	0.43	0	0	0	0
		4	0.02	0.3	Seq(DS1,DS2,DS3)		PIDR	3	7	62760	41840	0.28	36.9	24.6	0.37	0	0	0	0
Post-Northridge welded moment connection other than RBS (beams both sides, beam depth ≤ W27)	1 EA	1	0.03	0.3				3	7	62760	41840	0.28	36.9	24.6	0.37	0	0	0	0
		2	0.04	0.3	Seq(DS1,DS2,DS3)		PIDR	3	7	62760	41840	0.28	36.9	24.6	0.37	0	0	0	0
		3	0.05	0.3				3	7	70200	46800	0.25	41.3	27.5	0.35	0	0	0	0
		4	0.02	0.3	Seq(DS1,DS2,DS3)		PIDR	3	7	70200	46800	0.25	41.3	27.5	0.35	0	0	0	0
Buckling Restrained Brace (Chevron)	1 Bay	2	0.02	0.4	Seq(DS1)		Axial Strain	5	20	See Table S4	See Table S4	0.28	25	17	0.38	0	0	0	0
Curtain Walls	30 ft ²	1	0.034	0.4	Seq(DS1,DS2)		PIDR	20	100	2055	1096	0.17	0.9	0.5	0.30	0	0	0	0
Dry wall partition	100 ft	2	0.038	0.4				20	100	2055	1096	0.17	0.9	0.5	0.30	36	0.02	0	0.5
Dry wall finishes	100 ft	1	0.005	0.4				1	10	2678	1428	0.48	2.1	1.2	0.54	0	0	0	0
Prefabricated steel stair	1 EA	2	0.010	0.3	Seq(DS1,DS2,DS3)		PIDR	1	10	6825	3640	0.56	5.3	2.8	0.61	0	0	0	0
Raised access floor	100 ft ²	1	0.021	0.2				1	10	10500	7438	0.20	8.1	5.7	0.32	0	0	0	0
Suspended ceiling	250 ft ²	2	0.010	0.3	Seq(DS1,DS2,DS3)		PIDR	1	3	3240	2160	0.15	3.0	2.0	0.29	0	0	0	0
Independent pendant lighting	1 EA	1	0.05	0.4	Seq(DS1)		PFA	5	10	990	297	0.64	1.0	0.3	0.68	0	0	0	0
Cold or hot potable water piping (diameter ≤ 2.5 inches)	1000 ft	1	1.17g	0.25			PFA	1	4	319	261	0.76	0.3	0.3	0.80	0	0	0	0
Fire sprinkler water piping	1000 ft	2	2.06g	0.4	Seq(DS1,DS2)		PFA	1	4	2915	2385	0.41	0.6	0.1	0.48	0	0	0	0
Fire sprinkler drops	100 EA	1	1.17g	0.4	Seq(DS1,DS2)		PFA	2	5	385	315	0.65	0.5	0.4	0.70	0	0	0	0
HVAC ducting (cross sectional area ≥ 6 sf)	1000 ft	2	2.06g	0.4	Seq(DS1,DS2)		PFA	1	5	550	450	0.37	0.2	0.1	0.44	0	0	0	0
HVAC ducting (cross sectional area < 6 sf)	1000 ft	1	1.17g	0.4	Seq(DS1,DS2)		PFA	1	5	715	585	0.37	0.8	0.7	0.44	0	0	0	0
HVAC drops	10 EA	1	1.17g	0.4	Seq(DS1)		PFA	1	5	3300	2700	0.21	3.9	3.2	0.32	4	0.1	0	0.5
Variable Air Volume box	10 EA	1	1.17g	0.4	Seq(DS1)		PFA	1	5	16500	13500	0.29	19.4	15.9	0.39	0	0	0	0
Traction elevator	1 EA	2	0.39g	0.45	Simul(DS1,DS2,DS3,DS4)		PGA	5	10	37400	11220	0.28	35.8	10.7	0.37	0	0	0	0
Chiller	75 ton	1	0.2g	0.4	Seq(DS1)		PFA	1	5	50820	41580	0.18	14.3	4.8	0.31	0	0	0	0
Low voltage switchgear	225 AP	1	1.28g	0.4	Seq(DS1)		PFA	1	5	10202.5	8347.5	0.16	3.3	1.1	0.30	0	0	0	0
Motor control center	1 EA	1	0.73g	0.45	Seq(DS1)		PFA	1	5	4565	3735	0.18	2.0	1.0	0.31	0	0	0	0
Concrete tile roof	100 ft ²	1	1.1g	0.4	Seq(DS1,DS2)		PFA	13	130	840	490	0.58	1.0	0.6	0.63	0	0	0	0
Cooling tower	75 ton	1	1.0g	0.5	Seq(DS1)		PFA	1	5	26070	21330	0.17	8.4	2.8	0.30	0	0	0	0
Air handling unit	4000 CFM	1	0.25g	0.4	MutEx(DS1,DS2)		PFA	1	5	32120	26280	0.17	10.3	3.4	0.30	0	0	0	0

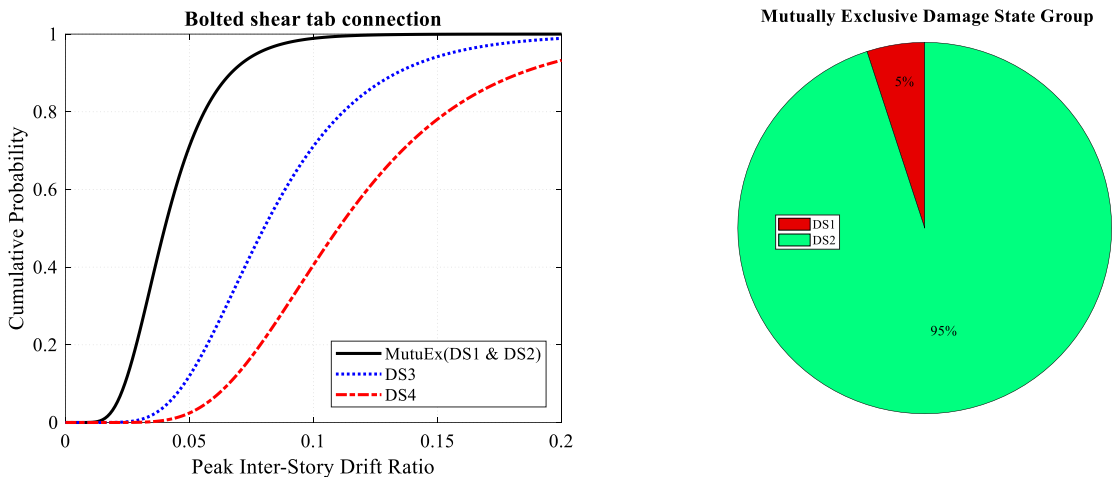
^a Damage fragility and consequence models for selected components are extracted from the FEMA P-58 fragility database [6].

^b DS: Damage State, Seq: Sequential, MutEx: Mutually Exclusive, Simul: Simultaneous, PIDR: Peak Intert-story Drift Ratio, PFA: Peak Floor Acceleration, PGA: Peak Ground Acceleration, β : Log-normal Standard Deviation, μ : Mean.

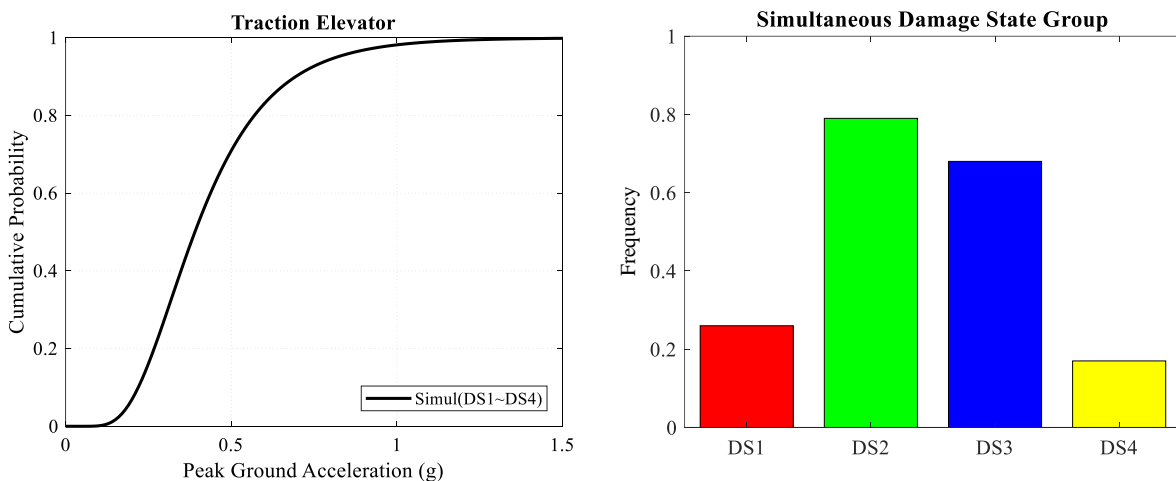
^c EA: per unit, AP: Amper, CFM: ft³/minute, 1 ft = 0.305 m.



(a) Sequential Damage State



(b) Mutually Exclusive Damage State



(c) Simultaneous Damage State

Fig. S4: Different samples of damage fragility models in vulnerable components: (a) welded moment connection, (b) bolted shear tab connection, and (c) traction elevator

Table S4: Details of repair cost and repair time for buckling-restrained braces in this study

Items	Quantity ^a	Unit Cost (\$)	Repair Cost (\$)	Repair Time (day-person)
Demolition and relocation:				
Partitions obstructing works (full height)	338 ft ²	3 \$/ft ²	1,014	1
Mechanical and electrical relocations as required for repair work	1	600 \$	600	1
Remove, store and reinstall:				
Ceilings	260 ft ²	8 \$/ft ²	2,080	2
Mechanical and electrical systems	1	600 \$	600	1
Office furniture and equipment	1	600 \$	600	1
Temporary:				
Floor protection (access)	1	1000 \$	1,000	1
Dust curtains	338 ft ²	3 \$/ft ²	1,014	1
Scaffolding or work platforms (underside access)	1	1500 \$	1,500	1
Shoring	1	2500 \$	2,000	1
Heat protection	1	500 \$	500	1
Replace:				
Partitions removed - patch in	338 ft ²	20	6,760	2
Fireproofing reapplication	1	600	600	1
Chevron BRB elements and gusset plates	1 Bay	BRBCost (Eq. (23))	2×BRBCost	7
Total:				
	Mean		18,268 + 2×BRBsCost	21
	Max.		1.2×Mean	25
	Min.		0.8×Mean	17

^a for Bay length = 20 ft (6.1 m), Story height = 13 ft (4.0 m), Clearance each side = 3 ft (0.9 m), 1 ft = 0.305 m,

Supplementary Details of Nonlinear Modeling

This section presents the calculation method of nonlinear modeling parameters of beam, column, and BRB, as well as their validation in OpenSees [7], as discussed in Section 3.2 of the paper.

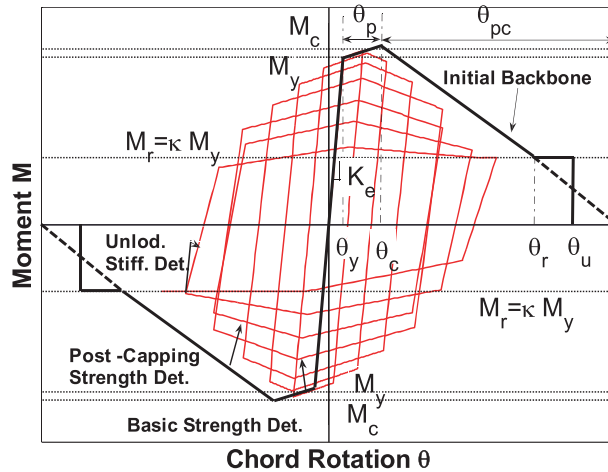


Fig. S5: IMK material model for defining the hysteretic behavior of steel beams and columns [8]

Table S5: Calculation method of IMK model parameters for wide-flange steel beams

Parameter	Value	Reference	Variables Definition
$K_e = \frac{6EI}{L}$, $K_{bc} = \frac{n+1}{n} K_e$, $K_{e,s} = nK_{bc}$		Ibarra and Krawinkler 2005 [9]	K_e : elastic stiffness of beam members per Fig. S5 K_{bc} : stiffness of elastic beam-column element $K_{e,s}$: elastic stiffness of beam plastic hinge n : ratio of the elastic stiffness of the plastic hinge to the stiffness of the elastic element E : Young's modulus of steel material I : beam moment of inertia L : beam length
$M_y = 1.2ZR_yF_y$		NIST 2017 [10]	M_y : effective flexural yield strength per Fig. S5 Z : plastic modulus of the beam cross-section R_y : expected-to-nominal yield stress ratio F_y : nominal yield stress
$M_c = 1.1M_y$		NIST 2017 [10]	M_c : peak flexural strength per Fig. S5
$M_r = 0.4M_y$		NIST 2017 [10]	M_r : residual flexural strength per Fig. S5
$\theta_p = 0.07 \left(\frac{h}{t_w} \right)^{-0.3} \left(\frac{b_f}{2t_f} \right)^{-0.1} \left(\frac{L}{d} \right)^{0.3} \left(\frac{c_{unit}d}{533} \right)^{-0.7}$		NIST 2017 [10]	θ_p : pre-peak plastic rotation per Fig. S5 θ_{pc} : post-peak plastic rotation per Fig. S5 θ_u : ultimate rotation capacity per Fig. S5 Λ : cyclic deterioration parameter h/t_w : web depth-to-thickness ratio $b_f/2t_f$: flange width-to-thickness ratio L/d : span-to-depth ratio of the beam d : beam depth L_d/r_y : ratio of the beam's unbraced length to minor axis radius of gyration c_{unit} : coefficient for unit conversion
$\theta_u = 0.2$		NIST 2017 [10]	
$\Lambda = \begin{cases} 495 \left(\frac{h}{t_w} \right)^{-1.34} \left(\frac{b_f}{2t_f} \right)^{-0.595} \left(\frac{c_{unit}F_y}{355} \right)^{-0.360} & \text{if } d \leq 533 \text{ mm (21in)} \\ 536 \left(\frac{h}{t_w} \right)^{-1.26} \left(\frac{b_f}{2t_f} \right)^{-0.525} \left(\frac{L_b}{r_y} \right)^{-0.130} \left(\frac{c_{unit}F_y}{355} \right)^{-0.291} & \text{if } d > 533 \text{ mm (21in)} \end{cases}$		Lignos and Krawinkler 2011 [11]	

Table S6: Calculation method of IMK model parameters for wide-flange steel columns

Parameter	Value	Reference	Variables Definition
$K_e = \frac{6EI_e}{L}$, $K_{bc} = \frac{n+1}{n} K_e$, $K_{e,s} = n K_{bc}$		Lignos et al. 2019 [12]	K_e : elastic stiffness of column member per Fig. S5 K_{bc} : stiffness of elastic beam-column element $K_{e,s}$: elastic stiffness of column plastic hinges n : ratio of the elastic stiffness of the plastic hinge to the stiffness of the elastic beam-column element E : Young's modulus of steel material G : shear modulus of the steel material I : effective moment of inertia I : column moment of inertia K_s : shear stiffness of the column K_b : flexural stiffness of the column A_w : web area of the wide-flange section L : column length
$I_e = \frac{K_s}{K_s + K_b} I$; $K_s = \frac{GA_w}{L}$, $K_b = \frac{12EI}{L^3}$		Lignos et al. 2019 [12]	
$M_y = \begin{cases} 1.15ZR_y F_y \left(1 - \frac{P_g}{2P_{ye}}\right) & \text{if } P_g / P_{ye} < 0.2 \\ 1.15ZR_y F_y \times \frac{9}{8} \left(1 - \frac{P_g}{P_{ye}}\right) & \text{if } P_g / P_{ye} \geq 0.2 \end{cases}$		Lignos et al. 2019 [12]	
$M_c = aM_y$; $a = 12.5 \left(\frac{h}{t_w}\right)^{-0.2} \left(\frac{L_b}{r_y}\right)^{-0.4} \left(1 - \frac{P_g}{P_{ye}}\right)^{0.4}$, $1.0 \leq a \leq 1.3$		Lignos et al. 2019 [12]	
$M_r = \left(0.5 - 0.4 \frac{P_g}{P_{ye}}\right) M_y$		Lignos et al. 2019 [12]	
$\theta_p = 294 \left(\frac{h}{t_w}\right)^{-1.7} \left(\frac{L_b}{r_y}\right)^{-0.7} \left(1 - \frac{P_g}{P_{ye}}\right)^{1.6} \leq 0.2$		Lignos et al. 2019 [12]	
$\theta_{pc} = 90 \left(\frac{h}{t_w}\right)^{-0.8} \left(\frac{L_b}{r_y}\right)^{-0.8} \left(1 - \frac{P_g}{P_{ye}}\right)^{2.5} \leq 0.3$		Lignos et al. 2019 [12]	
$\theta_u = 0.15$		Lignos et al. 2019 [12]	
$\Lambda = \begin{cases} 25500 \left(\frac{h}{t_w}\right)^{-2.14} \left(\frac{L_b}{r_y}\right)^{-0.53} \left(1 - \frac{P_g}{P_{ye}}\right)^{4.92} \leq 3.0 & \text{if } P_g / P_{ye} \leq 0.35 \\ 268000 \left(\frac{h}{t_w}\right)^{-2.30} \left(\frac{L_b}{r_y}\right)^{-1.30} \left(1 - \frac{P_g}{P_{ye}}\right)^{1.19} \leq 3.0 & \text{if } P_g / P_{ye} > 0.35 \end{cases}$		Lignos et al. 2019 [12]	

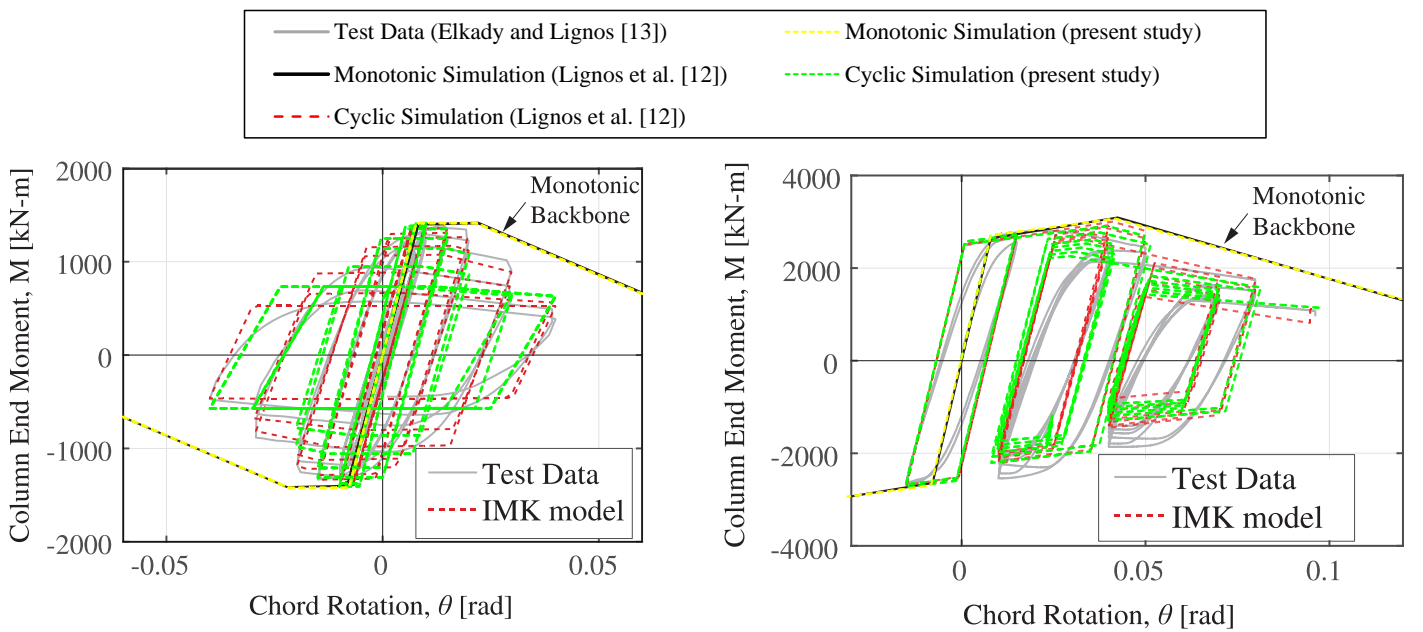


Fig. S6: Validation of IMK material model through comparison with full-scale laboratory tests: (a) for W24x84 steel column and (b) for W24x146 steel column

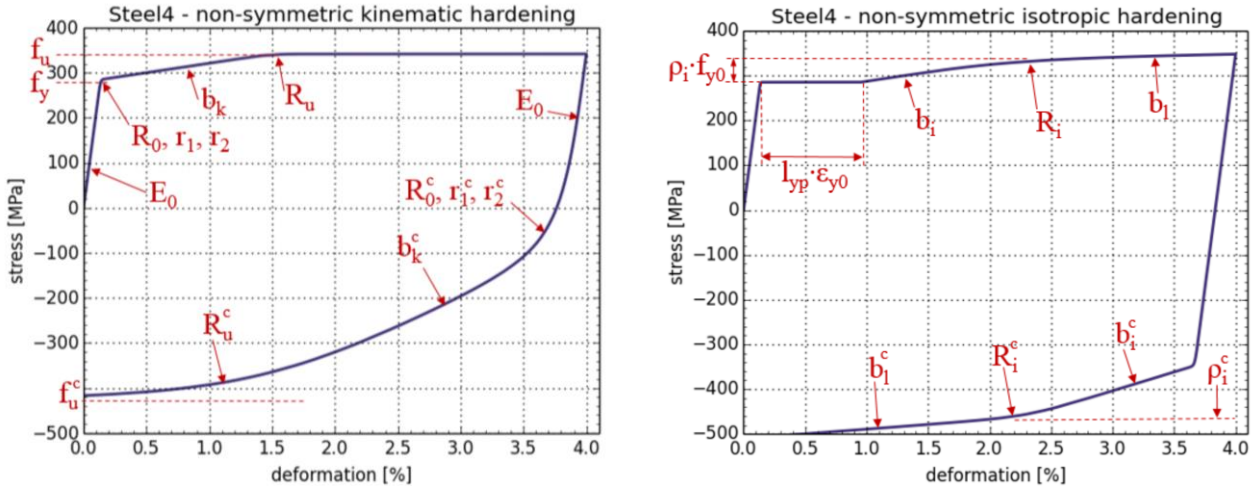


Fig. S7: Steel4 material model for defining the overall hysteretic behavior of BRBs [14]

Table S7: Calculation method of BRB material parameters [15]

BRB Material Parameter	Tension	Compression	Variables Definition
Steel4			
E_0		f_{SME}	E_0 : initial stiffness (Young's modulus) of steel core per Fig. S7
F_y		$R_y F_y$	f_{SM} : stiffness modification factor per Eq. (24) of the paper
kinematic hardening			
b_k	0.005	$0.03 - 0.005 \times f_A$	E : Young's modulus of steel material
R_0	25.0	25.0	F_y : yield strength of steel core
r_1	0.91	0.89	R_y : expected-to-nominal yield stress ratio
r_2	0.10	0.02	b_k : hardening ratio per Fig. S7
isotropic hardening			
b_i	$0.003 - 0.0005 \times f_A$	$0.005 + 0.001 \times f_A$	R_0, r_1, r_2 : parameters that describe exponential transition from linear elastic to hardening behavior per Fig. S7
b_l	0.0001	$0.0004 - 0.00007 \times f_A$	b_i : initial hardening ratio per Fig. S7
p_i		$0.25 + 0.05 \times f_A$	b_l : saturated hardening ratio per Fig. S7
R_i		3.0	p_i : a parameter that specifies the position of the intersection point between initial and saturated hardening asymptotes per Fig. S7
l_{yp}		1.0	R_i : a parameter that controls the exponential transition from initial to saturated asymptote per Fig. S7
ultimate strength limit			
F_u	$1.65 F_y$	$2.40 F_y$	l_{yp} : a parameter that controls the length of the yielding plateau per Fig. S7
R_u		2.0	F_u : ultimate strength of steel core
Fatigue			
m		-0.400	R_u : a parameter that controls the exponential transition from kinematic hardening to perfectly plastic asymptote per Fig. S7
ε_0		$(0.14 + 0.4 \times (R_y - 1.1)) / f_{DM}$	m : fatigue exponent
			ε_0 : parameters that describe strength deterioration due to low cycle fatigue
			$f_A = \sqrt{A_{yz} [\text{mm}^2] / 5000}$
			$f_{DM} = L_{wp} / L_{yz}$
			A_{yz} : yield zone area of steel core
			L_{wp} : workpoint-to-workpoint length of BRB
			L_{yz} : yield zone length of steel core

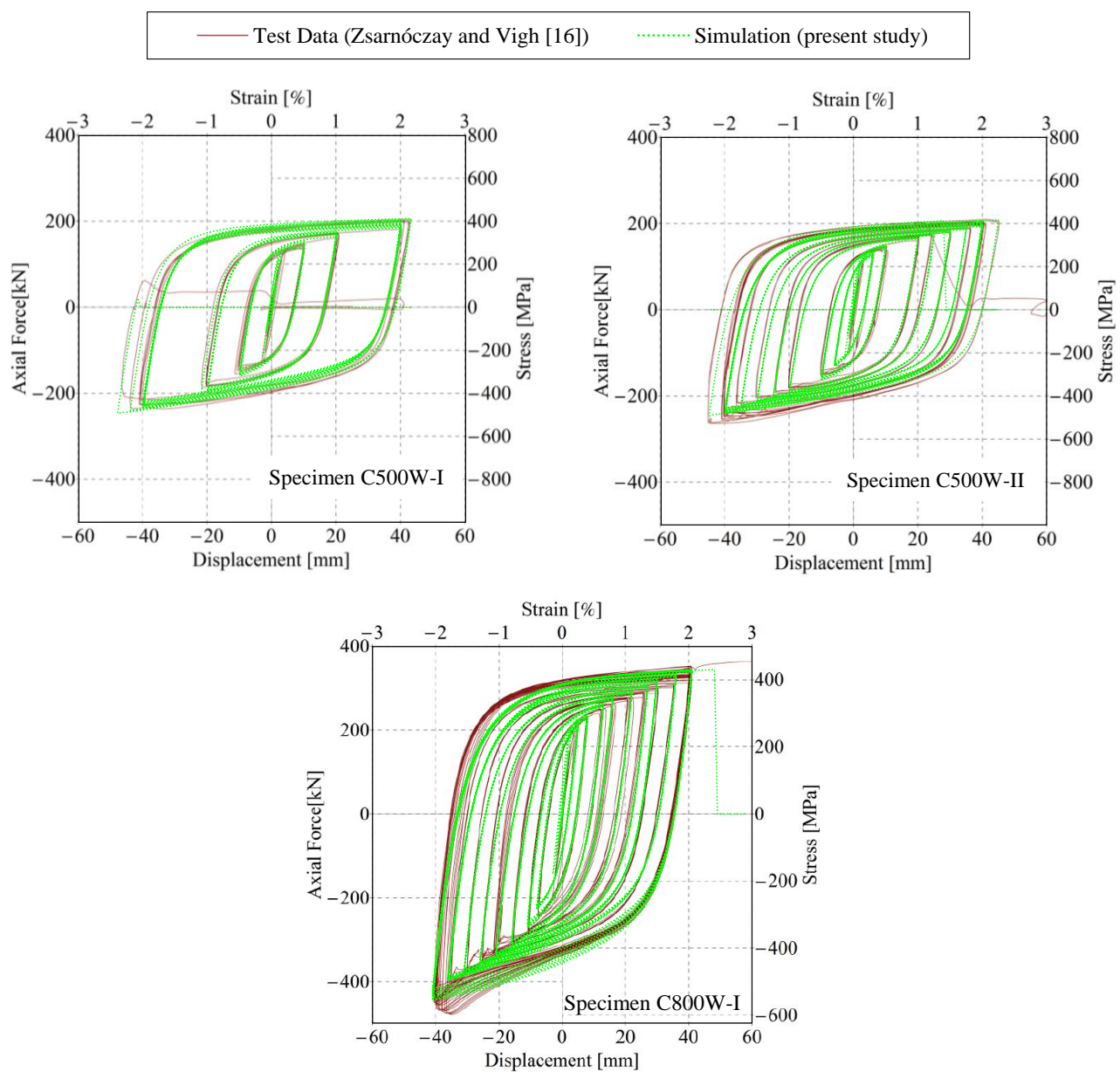


Fig. S8: Validation of BRB material model in OpenSees through comparison with full-scale laboratory tests

Supplementary Figures

This section presents supplementary figures that are referenced in the paper.

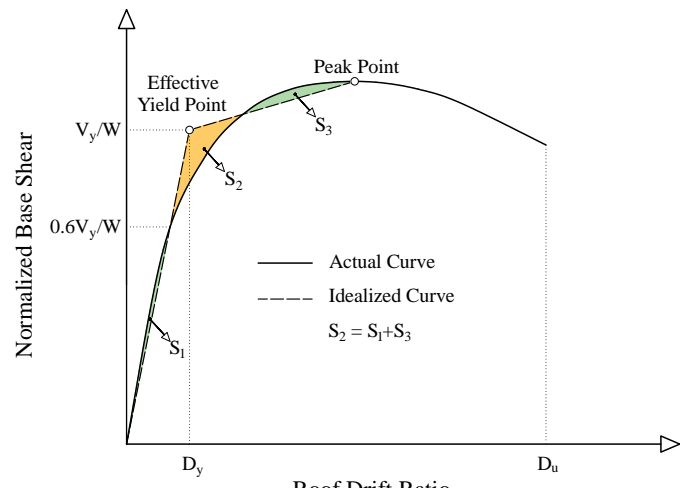


Fig. S9: Idealization of the capacity curve based on ASCE41-17 [17]

Endurance Time Analysis Validation

This section of the supplementary document validates the results of the Endurance Time Analysis (ETA) [18] of LCC-based optimized SMRF-BRBs discussed in Section 3.4 of the paper. The benchmark method here is Incremental Dynamic Analysis (IDA) [19] under natural ground motions, as recommended in FEMA P-58 [5]. For this purpose, 22 pairs of far-field ground motions suggested by FEMA P695 [20] are used as shown in Table S8. These ground motions comprise strong-motion records of stiff soil and soft rock sites with dominant strike-slip and thrust mechanisms whose moment magnitude varies between 6.5 and 7.6 and have been recorded at an epicentral distance of at least 8.7 kilometers from fault rupture. Fig. S10 shows the acceleration spectrum of these records without scaling. According to FEMA P695, to scale ground motion records to a specific intensity level in the IDA process, each record is first normalized based on the peak ground velocity ratio. The normalized records are then scaled so that their median spectral acceleration equals the target spectral acceleration for the specified intensity level in the fundamental period of the building. Figs. S11-S17 and Tables S9 and S10 compare the results obtained with the IDA and ETA methods. As can be seen, the ETA method predicts IDA results with acceptable accuracy, which corroborates the validity of the conclusions reached in the paper.

Table S8: Properties of the FEMA P695 far-field ground motions set used in this study

Pair No.	Earthquake Name	Year	Magnitude	Station Name	Fault Type	Site Class	Distance (km) ^a	PGA _{max} (g) ^b
1	Northridge	1994	6.7	Beverly Hills - Mulhol	Thrust	D	13.3	0.52
2	Northridge	1994	6.7	Canyon Country-WLC	Thrust	D	26.5	0.48
3	Duzce, Turkey	1999	7.1	Bolu	Strike-slip	D	41.3	0.82
4	Hector Mine	1999	7.1	Hector	Strike-slip	C	26.5	0.34
5	Imperial Valley	1979	6.5	Delta	Strike-slip	D	33.7	0.35
6	Imperial Valley	1979	6.5	El Centro Array #11	Strike-slip	D	29.4	0.38
7	Kobe, Japan	1995	6.9	Nishi-Akashi	Strike-slip	C	8.7	0.51
8	Kobe, Japan	1995	6.9	Shin-Osaka	Strike-slip	D	46	0.24
9	Kocaeli, Turkey	1999	7.5	Duzce	Strike-slip	D	98.2	0.36
10	Kocaeli, Turkey	1999	7.5	Arcelik	Strike-slip	C	53.7	0.22
11	Landers	1992	7.3	Yermo Fire Station	Strike-slip	D	86	0.24
12	Landers	1992	7.3	Coolwater	Strike-slip	D	82.1	0.42
13	Loma Prieta	1989	6.9	Capitola	Strike-slip	D	9.8	0.53
14	Loma Prieta	1989	6.9	Gilroy Array #3	Strike-slip	D	31.4	0.56
15	Manjil, Iran	1990	7.4	Abbar	Strike-slip	C	40.4	0.51
16	Superstition Hills	1987	6.5	El Centro Imp. Co.	Strike-slip	D	35.8	0.36
17	Superstition Hills	1987	6.5	Poe Road (temp)	Strike-slip	D	11.2	0.45
18	Cape Mendocino	1992	7	Rio Dell Overpass	Thrust	D	22.7	0.55
19	Chi-Chi, Taiwan	1999	7.6	CHY101	Thrust	D	32	0.44
20	Chi-Chi, Taiwan	1999	7.6	TCU045	Thrust	C	77.5	0.51
21	San Fernando	1971	6.6	LA - Hollywood Stor	Thrust	D	39.5	0.21
22	Friuli, Italy	1976	6.5	Tolmezzo	Thrust	C	20.2	0.35

^a Epicentral site-source distance

^b Maximum amount of two horizontal components

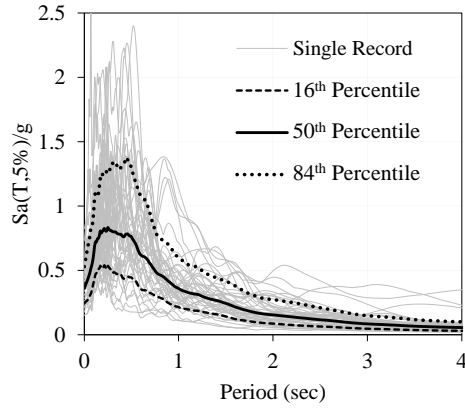


Fig. S10: The acceleration spectrum of 44 unscaled far-field records of FEMA P695

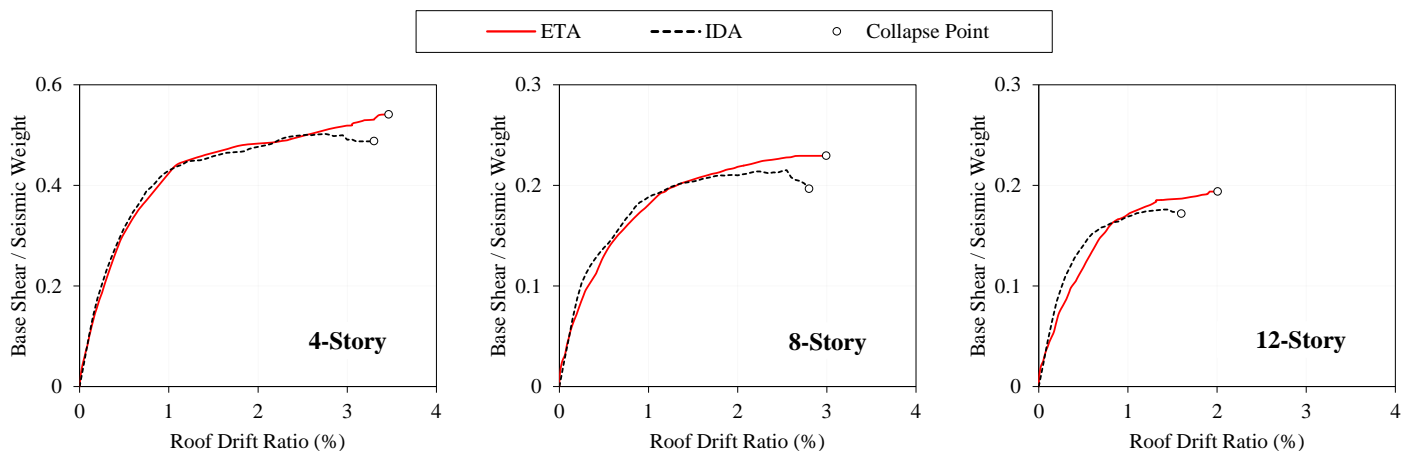


Fig. S11: Comparison of the ETA and IDA methods for determining dynamic capacity curves of LCC-based optimized buildings

Table S9: Comparison of the ETA and IDA methods for determining key parameters related to the overall seismic behavior of LCC-based optimized buildings

Parameters	4-Story		8-Story		12-Story	
	IDA	ETA	IDA	ETA	IDA	ETA
Normalized Effective Yield Strength, V_y/W	0.424	0.408	0.183	0.190	0.1593	0.1587
Normalized Maximum Strength, V_{max}/W	0.502	0.541	0.215	0.229	0.176	0.194
Effective Yield Roof Drift, D_y (%)	0.583	0.600	0.500	0.704	0.417	0.578
Ultimate Roof Drift, D_u (%)	3.300	3.466	2.800	2.994	1.600	2.007

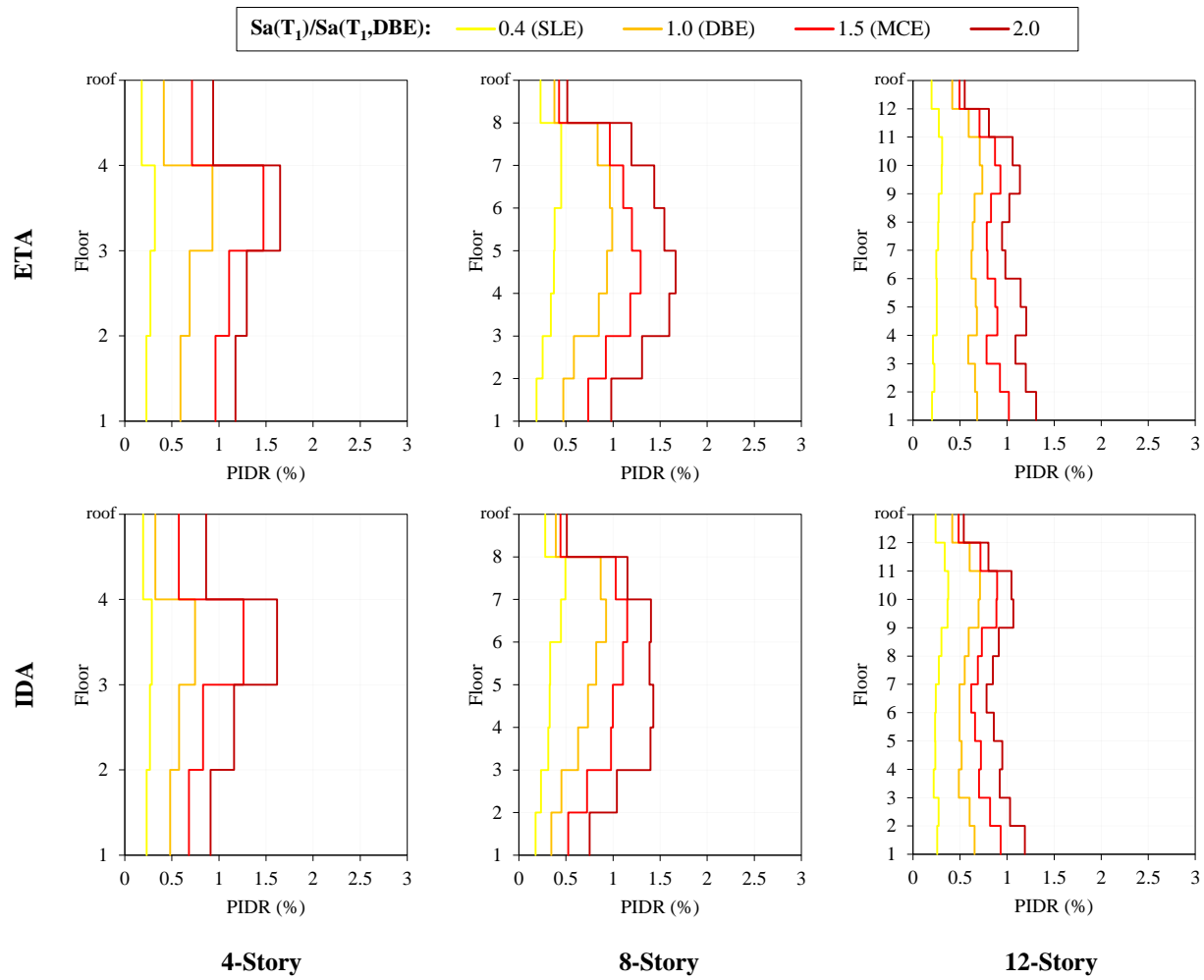


Fig. S12: Comparison of the ETA and IDA methods for determining the median of the PIDR response profile of LCC-based optimized buildings at various seismic hazard levels

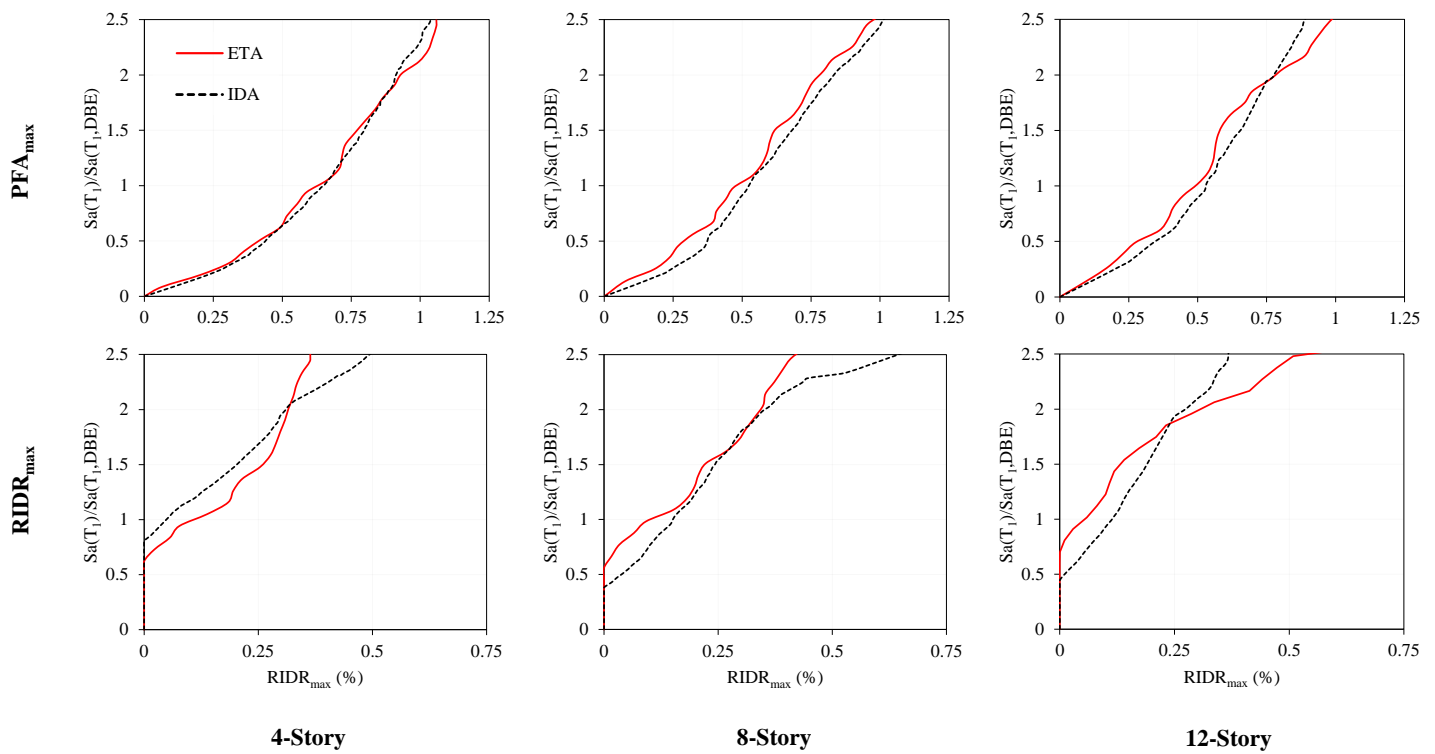


Fig. S13: Comparison of the ETA and IDA methods for determining the median of the PFA_{max} and $RIDR_{max}$ responses of LCC-based optimized buildings at various seismic hazard levels

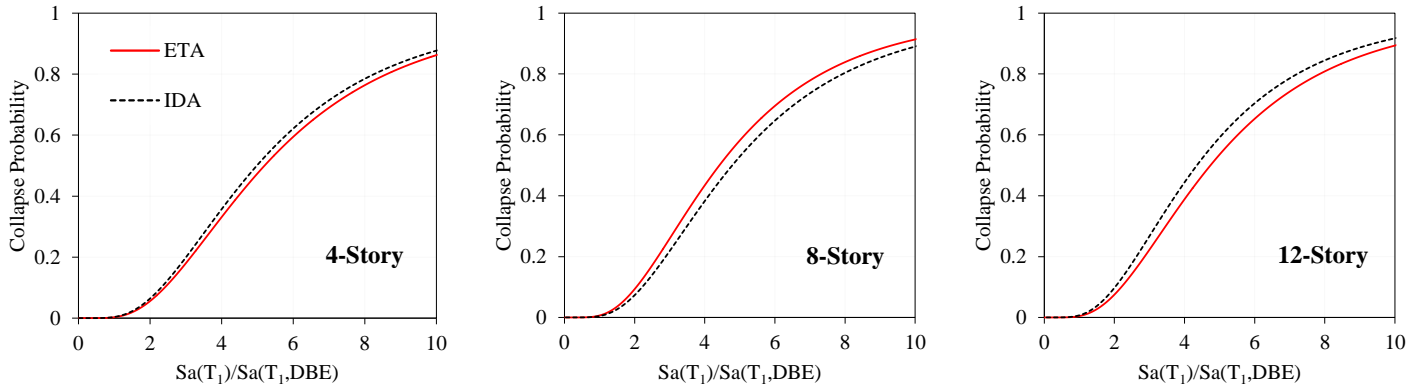


Fig. S14: Comparison of the ETA and IDA methods for determining collapse fragility curves of LCC-based optimized buildings

Table S10: Comparison of the ETA and IDA methods for quantifying target safety indices of LCC-based optimized buildings

Target Safety Indices	4-Story		8-Story		12-Story		Average	
	IDA	ETA	IDA	ETA	IDA	ETA	IDA	ETA
Collapse Probability at MCE	2.26%	1.91%	2.65%	3.59%	3.81%	2.76%	2.91%	2.75%
Annual Collapse Rate, λ_c	0.47E-04	0.40E-04	0.55E-04	0.74E-04	0.78E-04	0.57E-04	0.6E-04	0.57E-04
50-year Collapse Probability, P_c	0.24%	0.20%	0.28%	0.37%	0.39%	0.28%	0.30%	0.28%
50-year Reliability Index, β	2.82	2.88	2.77	2.68	2.66	2.77	2.75	2.78

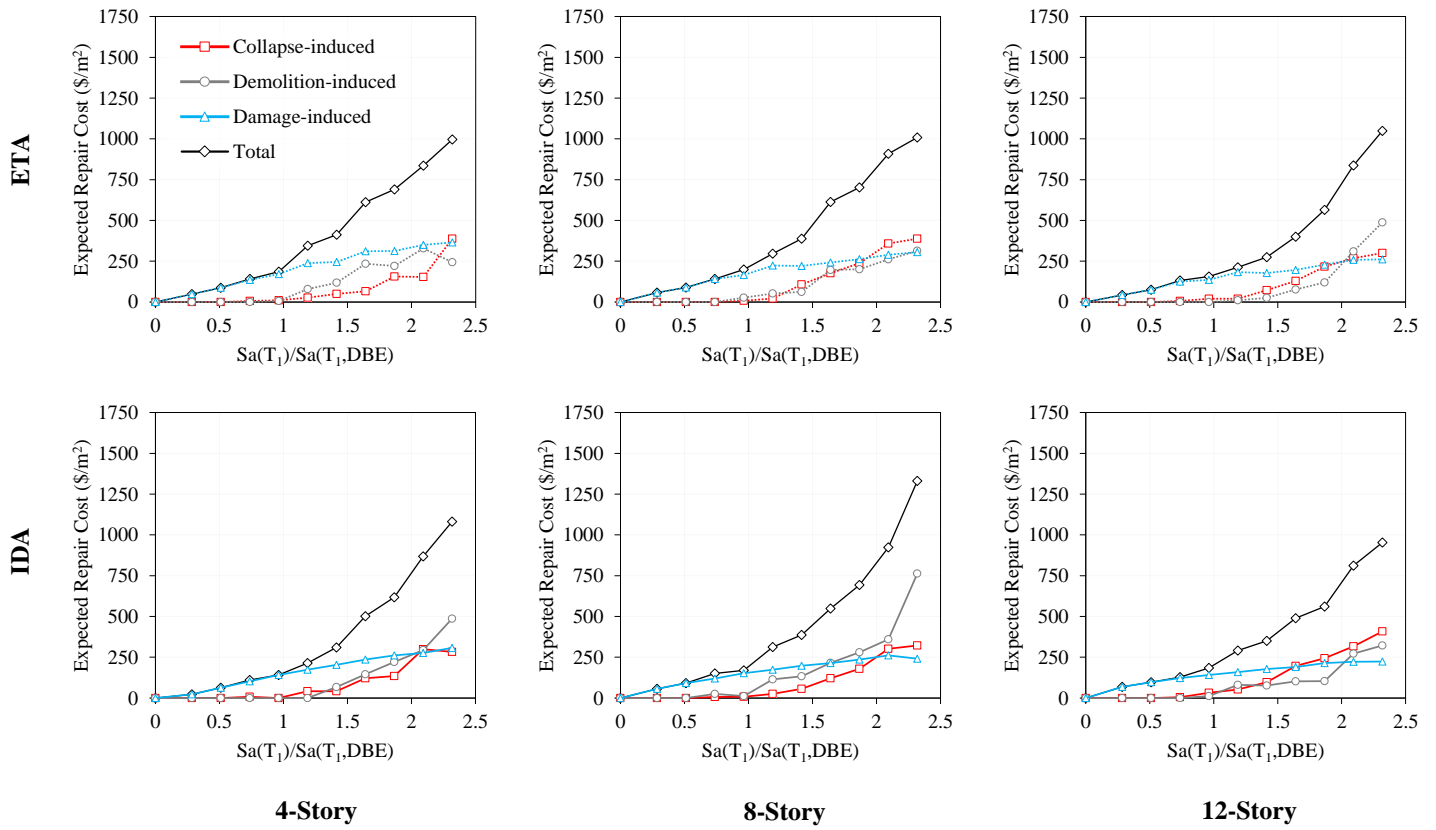


Fig. S15: Comparison of the ETA and IDA methods for estimating expected repair cost conditioned on seismic intensity in LCC-based optimized buildings

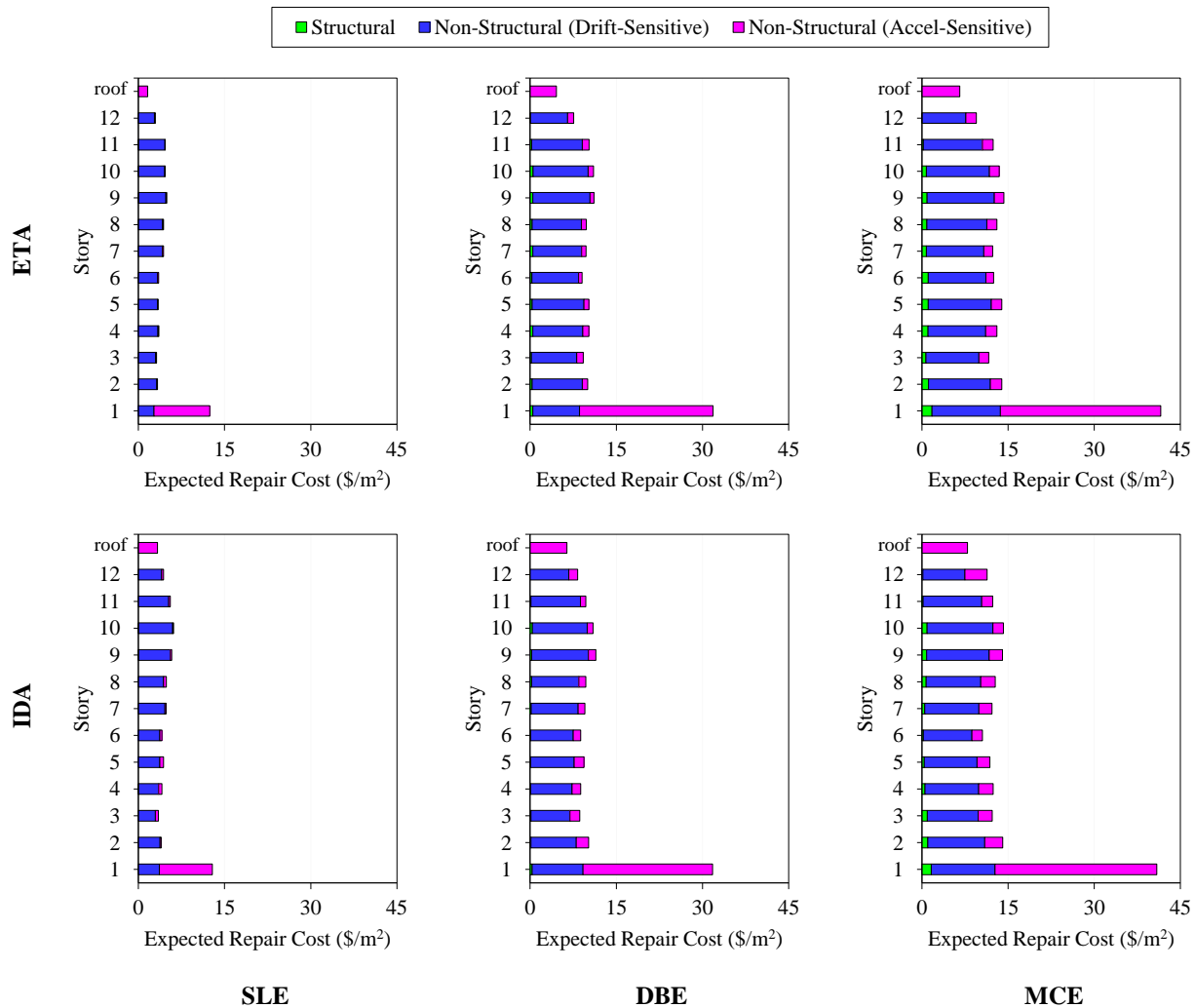


Fig. S16: Comparison of the ETA and IDA methods for estimating damage-induced expected repair cost profiles at various seismic hazard levels for the 12-story LCC-based optimized building

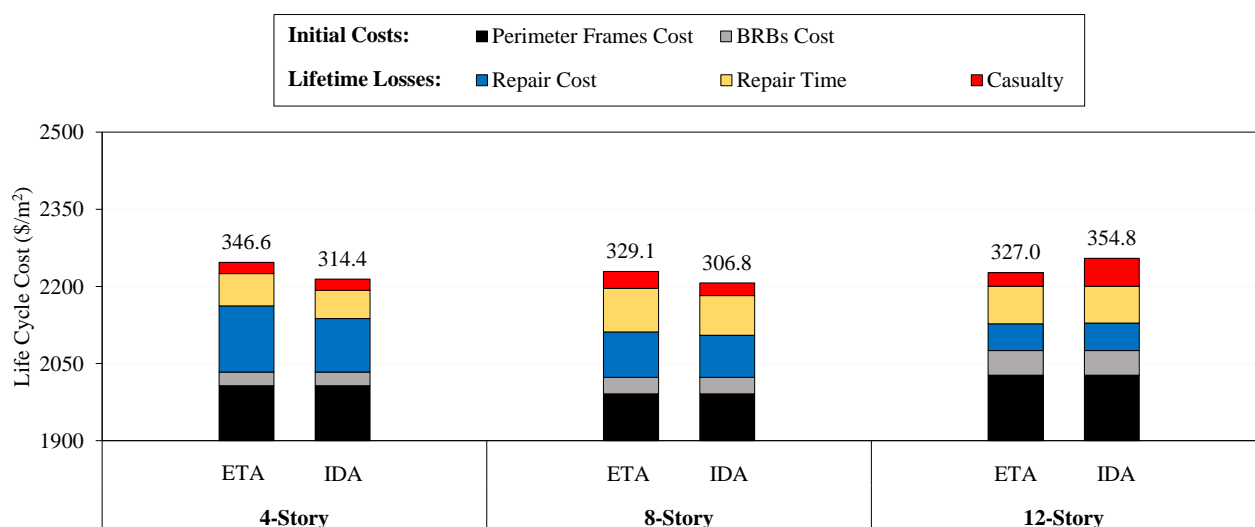


Fig. S17: Comparison of the ETA and IDA methods for estimating life cycle cost components of LCC-based optimized buildings

References

- [1] J. A. Jarrett, J. P. Judd, and F. A. Charney, Comparative evaluation of innovative and traditional seismic-resisting systems using the FEMA P-58 procedure, *Journal of Constructional Steel Research*, vol. 105, pp. 107-118, 2015. <http://doi.org/10.1016/j.jcsr.2014.10.001>.
- [2] CityFeet, Commercial Real Estate for Sale, Lease & Coworking Space, 2022, Available online at: www.cityfeet.com.
- [3] H. Shin and M. Singh, Minimum life-cycle cost-based optimal design of yielding metallic devices for seismic loads, *Engineering Structures*, vol. 144, pp. 174-184, 2017. <http://doi.org/10.1016/j.engstruct.2017.04.054>.
- [4] RSMeans, Square Foot Costs with RSMeans data, RSMeans Corporation: Kingston, MA. USA., 2016.
- [5] FEMA P-58-1, *Seismic Performance Assessment of Buildings*, Volume 1 - Methodology, Second Edition, Washington, DC: Federal Emergency Management Agency, 2018.
- [6] FEMA P-58-3, *Seismic Performance Assessment of Buildings* Volume 3 - Supporting Electronic Materials, Washington, DC: Federal Emergency Management Agency, 2018.
- [7] F. T. McKenna, Object-Oriented Finite Element Programming: Frameworks for Analysis, Algorithms, and Parallel Computing, Ph.D. dissertation, University of California at Berkeley, Berkeley, CA, 1999.
- [8] D. G. Lignos, H. Krawinkler, and A. S. Whittaker, Prediction and validation of sidesway collapse of two scale models of a 4-story steel moment frame, *Earthquake Engineering & Structural Dynamics*, vol. 40, no. 7, pp. 807-825, 2011. <http://doi.org/10.1002/eqe.1061>.
- [9] L. Ibarra and H. Krawinkler, Global Collapse of Frame Structures under Seismic Excitations, Report No. 152, John A. Blume Earthquake Engineering Center, Stanford, California, 2005.
- [10] NIST, *Recommended Modeling Parameters and Acceptance Criteria for Nonlinear Analysis in Support of Seismic Evaluation, Retrofit, and Design*, NIST GCR 17-917-45, prepared by the Applied Technology Council for the National Institute of Standards and Technology, Gaithersburg, Maryland, April 2017. <https://doi.org/10.6028/NIST.GCR.17-917-45>.
- [11] D. G. Lignos and H. Krawinkler, Deterioration modeling of steel components in support of collapse prediction of steel moment frames under earthquake loading, *Journal of Structural Engineering-Reston*, vol. 137, no. 11, p. 1291, 2011. [http://doi.org/10.1061/\(ASCE\)ST.1943-541X.0000376](http://doi.org/10.1061/(ASCE)ST.1943-541X.0000376).
- [12] D. Lignos, A. R. Hartloper, A. M. A. Elkady, G. G. Deierlein, and R. Hamburger, Proposed updates to the ASCE 41 nonlinear modeling parameters for wide-flange steel columns in support of performance-based seismic engineering, *Journal of Structural Engineering*, vol. 145, p. 04019083, 2019. [http://doi.org/10.1061/\(ASCE\)ST.1943-541X.0002353](http://doi.org/10.1061/(ASCE)ST.1943-541X.0002353).
- [13] A. M. A. Elkady and D. Lignos, Full-scale testing of deep wide-flange steel columns under multiaxis cyclic loading: Loading sequence, boundary effects, and lateral stability bracing force demands, *Journal of Structural Engineering*, vol. 144, no. ARTICLE, p. 04017189, 2018. [http://doi.org/10.1061/\(ASCE\)ST.1943-541X.0001937](http://doi.org/10.1061/(ASCE)ST.1943-541X.0001937).
- [14] University of California, Berkeley, Pacific Earthquake Engineering Research Centre; 2016, Available online at: https://opensees.berkeley.edu/wiki/index.php/Steel4_Material.
- [15] Á. Zsarnóczay and L. G. Vigh, Eurocode conforming design of BRBF–Part II: Design procedure evaluation, *Journal of Constructional Steel Research*, vol. 135, pp. 253-264, 2017. <http://doi.org/10.1016/j.jcsr.2017.04.013>.
- [16] A. Zsarnoczay, Experimental and numerical investigation of buckling restrained braced frames for Eurocode conform design procedure development, Ph.D. dissertation, Budapest University of Technology and Economics, 2013.
- [17] ASCE/SEI 41-17, *Seismic evaluation and retrofit of existing buildings*, Reston, VA: American Society of Civil Engineers, 2017.

- [18] H. Ahmadie Amiri, M. Hosseini, and H. E. Estekanchi, Efficient seismic risk assessment of irregular steel-framed buildings through endurance time analysis of consistent fish-bone model, *The Structural Design of Tall and Special Buildings*, vol. 31, no. 2, 2021. <http://doi.org/10.1002/tal.1901>.
- [19] D. Vamvatsikos and C. A. Cornell, Incremental dynamic analysis, *Earthquake engineering & structural dynamics*, vol. 31, no. 3, pp. 491-514, 2002. <http://doi.org/10.1002/eqe.141>.
- [20] FEMA P695, *Quantification of Building Seismic Performance Factors*, Washington, DC: Federal Emergency Management Agency, 2009.